Time-Dependent Density Functional Theory Calculations of Ligand K Edge and Metal L Edge X-ray Absorption of a Series of Oxomolybdenum Complexes

G. Fronzoni,* M. Stener, A. Reduce, and P. Decleva

Dipartimento di Scienze Chimiche, Università di Trieste, Via L. Giorgieri 1, I-34127 Trieste, Italy, and Consorzio Interuniversitario Nazionale per la Scienza e Tecnologia dei Materiali, INSTM, Unita' di Trieste, and INFM DEMOCRITOS National Simulation Center, Trieste, Italy

Received: May 13, 2004; In Final Form: July 22, 2004

X-ray absorption spectra (XAS) at the Cl and S K edge and Mo L edge have been calculated at the TDDFT level for a series of dioxomolybdenum complexes $LMoO_2X$ (L = hydrotris(3,5-dimethyl-1-pyrazolyl)borate, X = Cl, SCH_2Ph, OPh), which play an important role in modeling the catalytic cycle of the sulfite oxidase enzyme. Also, the XAS spectra of model molecules of the Mo complexes have been simulated and interpreted in terms of the Mo 4d orbital splitting, in order to find possible correlations with the spectral pattern of the complexes. Comparison with the available experimental data allows us to assess the performances of the present computational scheme to describe the core excitations in large bioinorganic systems. The theoretical interpretation of the spectral features of both the metal and ligand core excitations in terms of the oscillator strength distribution provides important insight into the covalency of the metal−ligand bond.

1. Introduction

Molybdenum is the only second-row transition metal known to be essential for living systems. Its active biological form, present in almost all Mo-containing enzymes, is known as molybdenum cofactor (Moco), and it appears that the coordination by this ligand is essential for the catalytic function of the Mo enzymes. The Mo active center is common to important human enzymes including xanthine oxidase, sulfite oxidase, and aldehyde oxidase. In particular, the sulfite oxidase enzyme catalyzes the conversion of sulfite to sulfate, the terminal step in the oxidative degradation of cysteine and methionine. Structural information on the coordination of Mo in the sulfite oxidase, provided by EXAFS[1] and crystal studies,[2] has revealed that in oxidized sulfite oxidase the Mo is pentacoordinated by three sulfur ligands and two oxo groups with approximate square pyramidal coordination geometry. Two of the sulfur ligands arise from the thiolene group of the molybdopterin unit, and the third is contributed by the side chain of a cysteine molecule:

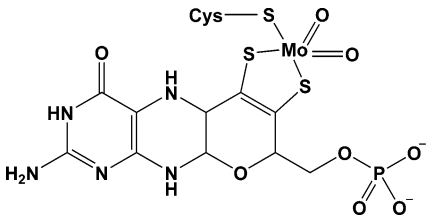

The conversion of sulfite to sulfate, catalyzed by sulfite oxidase, occurs with the transfer of an oxygen atom from the dioxo-Mo(VI) center of the enzyme to sulfite to generate an oxo-Mo(IV) center and sulfate. Important insight into the mechanism of the oxygen-atom transfer can be greatly facilitated by studies of the chemistry of inorganic models for the Mo cofactor, designed to mimic the MoO_2 center and simulate the cofactor ligand donor atom set. Among the several complexes investigated,[3] an especially significant model is based on a tris(pyrazolyl)borate ligand (L) which is able to catalyze the transfer of an oxygen atom from a suitable donor to an acceptor. It has been verified that a model of the form $LMoO_2X$, with X as the coligand, reacts in the oxidized form with PPh_3 (triphenyl phosphine), losing an oxo group which is then regenerated from water, therefore mimicking the key features of the catalytic cycle proposed for the sulfite oxidase.[4] A series of dioxo-Mo(VI) complexes of the type $LMoO_2X$ (L = hydrotris(3,5-dimethyl-1-pyrazolyl)borate, X = Cl, Br, OPh, SPh, SCH_2Ph, $SCH(CH_3)_2$) have been recently synthesized and characterized.[5] Electronic structure insight for these complexes has been obtained from the analysis of the pre-edge X-ray absorption spectra (XAS), which can provide useful information on the metal−ligand center covalency and its effects on the oxo transfer activity.[4]

It is well-known that XAS spectroscopy is one of the premier tools to elucidate the local structure environment of metal ions, even in low concentrations. XAS involves the photoexcitation of core electrons to unoccupied valence orbitals and to the continuum. Its great advantage is associated with the strongly localized nature of the core excitations, which makes the K and L edge spectra very sensitive to the electronic structure and to the local geometrical environment of the absorbing atom even when it is embedded in a very complex situation. XAS has been also applied to biological molecules,[6−8] providing important insight into the electronic characterization of the metalloproteins' active sites, which often exhibit unique spectroscopic features that reflect highly covalent sites. In particular, the metal L edge ($2p \rightarrow 3d$ + continuum) and the ligand K edge ($1s \rightarrow 3p$ + continuum) are particularly useful because of both the improved resolution of the experiments at lower energies and the electric-dipole-allowed nature of the transitions involved, which can give important information on the covalency of ligand−metal bonds.[9−11] In fact, the intensity of the metal L edge features provides a direct probe of the d metal contribution to the half-occupied or unoccupied valence antibonding MOs, whereas the intensity of the ligand K edge structures allows us to estimate the 3(*n*)p ligand character in these MOs due to covalent bonding.

10.1021/jp047953u CCC: $27.50
Published on Web 09/09/2004

Metal−ligand bonding in metallobiomolecules is dominated by the ligand's σ and π donor interactions, with neutral ligands behaving mostly as σ donors. The metal centers with d orbitals that are relatively high in energy can be available for π bonding interaction with the unoccupied low-lying valence orbitals on the neutral ligands. In some instances, ligand−metal donor interactions can be highly covalent, with the covalency greatly influencing the reactivity of the metal center.

Major advances have also been made in the field of theoretical approaches for the calculations of the electronic structure of large systems. In particular, the density functional theory (DFT) allows high-level calculations on large transition-metal systems, as required for metalloprotein active sites. Here, it should be emphasized that the detailed information obtainable from accurate calculations can be of significant support in the understanding of the virtual electronic states of the molecular system and in the assignment of the related measured spectral features. The time-dependent extension of the DFT (TDDFT) can be applied to electronic excited states, and from its origin, it has received a noteworthy impulse to describe optical absorption in atoms and molecules.[12,13] TDDFT represents the state of the art for evaluation of the molecular electronic transitions in the DFT framework. The current TDDFT implementations[14−17] allow the calculations of the outer valence excitation spectra in terms of excitation energies and oscillator strengths. Recently, an extension of the method in the ADF code[18] to the treatment of core excitations has been implemented, and test calculations of the XAS spectra of the $TiCl_4$ molecule have been performed at the K and L metal edges and ligand L edge, which gave excellent agreement between theory and experiment. It is important to underline that, at the TDDFT level also, the coupling between different excitation channels, which becomes allowed in the case of degenerate core holes (such as 2p), is included and proves to be very important in describing the 2p absorption edge. The results obtained have pointed out the reliability of the method to properly describe and interpret core excitation spectra, and its computational economy makes it a good candidate to treat larger and less symmetric systems with reasonable effort.

In this work, we present an application of the TDDFT method to the calculations of the ligand K edge and metal L edge of the Mo(VI) complexes $LMoO_2X$ (X = Cl, SCH_2Ph, OPh), which mimic the $[Mo^{VI}O_2]^{2+}$ active site of the sulfite oxidase enzyme. The comparison of the TDDFT results with the XAS experimental spectra measured by Izumi et al.[4] allows us to assess the performance of the present approach for simulation of the XAS spectra of large bioinorganic systems. The TDDFT calculations are also performed on the core excitations of model molecules for the three $LMoO_2X$ complexes in order to analyze in detail the electronic structure and the metal−ligand bond in simpler systems. The possibility to extend the estimate of metal−ligand covalency from the model analogous to the complex system through the comparison of their XAS spectra is pointed out.

2. Theoretical Method

The TDDFT approach for electron excitations and its implementation in the ADF code has been described in detail in the literature;[14,19] here, we just recall the salient steps and describe the new features. The general problem is cast in the following eigenvalue equation:

$$\mathbf{\Omega F}_i = \omega_i^2 \mathbf{F}_i \qquad (1)$$

where Ω is a four-index matrix with elements $\Omega_{ia\sigma,jb\tau}$, and the indexes consist of products of occupied virtual (*ia* and *jb*) KS orbitals, while σ and τ refer to the spin variable. The eigenvalues ω_i^2 correspond to squared excitation energies, while the oscillator strengths are extracted from the eigenvectors $\mathbf{F}_i$.[19] The Ω-matrix elements can be expressed in terms of KS eigenvalues (ϵ) and the coupling matrix *K*:

$$\Omega_{ia\sigma,jb\tau} = \delta_{\sigma\tau}\delta_{ij}\delta_{ab}(\epsilon_a - \epsilon_i)^2 + 2\sqrt{(\epsilon_a - \epsilon_i)}K_{ia\sigma,jb\tau}\sqrt{(\epsilon_b - \epsilon_j)} \qquad (2)$$

The elements of the coupling matrix *K* are given by the following expression:

$$K_{ij\sigma,kl\tau} = \int d\mathbf{r} \int d\mathbf{r}' \varphi_{i\sigma}(\mathbf{r})\varphi_{j\sigma}(\mathbf{r})\left[\frac{1}{|\mathbf{r} - \mathbf{r}'|} + f_{xc}^{\sigma\tau}(\mathbf{r}, \mathbf{r}', \omega)\right]\varphi_{k\tau}(\mathbf{r}')\varphi_{l\tau}(\mathbf{r}') \qquad (3)$$

where the φ's are the KS orbitals and $f_{xc}^{\sigma\tau}(\mathbf{r}, \mathbf{r}', \omega)$ is the exchange correlation kernel. In this work, the kernel is approximated according to the adiabatic local density approximation (ALDA).[20]

The space spanned by the solutions of eigenvalue eq 1 corresponds to the 1h−1p excited configurations, so it is possible to approximate this space operating a selection over the configurations, keeping only those necessary for an accurate description of the phenomenon, as is customary in ab initio CI calculations. So, in practice, according to the method in ref 18, the indexes which span the occupied orbital space (*i* and *j*) are limited to run only over the core shell.

3. Computational Details

The calculations have been performed with the ADF program,[21,22] modified according to the previous section. The all-electron triple-ζ plus polarization Slater-type orbitals (TZP STO) basis set has been used for all the atoms except hydrogen, for which the double-ζ (DZ) set without the polarization function has been chosen. All basis sets have been taken from the ADF database. The same tests previously performed with other basis sets have proven that the present choice is a good compromise between accuracy and computational effort.

The LB94[23] exchange correlation potential with the ground-state (GS) electron configuration has been employed. It has been chosen because of its correct asymptotic behavior, which is a necessary condition for a good description of virtual orbitals.

The exchange correlation kernel is approximated within the usual ALDA scheme, and only excitations with singlet spin symmetry have been considered.

In the model molecules, the nitrogen atoms of ligand L (reported in Chart 1) were replaced by three ammonia molecules, and the thiolate and alkoxide ligands were represented by SCH_3 and OCH_3, respectively (see Chart 1). For the geometry of the model molecules, the same strategy used in the work of Izumi et al.[4] has been adopted without any geometry optimization or symmetry idealization.

For the $LMoO_2X$ complexes, a DFT geometry optimization has been performed, employing the VWN potential[24] using a double-ζ plus polarization (DZP) basis set for B, C, N, and O, a DZ set for the Mo atom, and a single-ζ (SZ-STO) basis set for H. All core levels (up to 1s for B, C, N, and O; 2p for S and Cl; and 3d for Mo) have been treated as frozen orbitals. The calculated Mo−X distances are 2.31, 2.38, and 1.94 Å for X = Cl, SCH_2Ph, and OPh, respectively, which are found in

CHART 1: Coordinate Systems Used in the DFT Calculations for the Model Molecules $[(NH_3)_3MoO_2X]^+$ (X = Cl, SCH_3, OCH_3) (Upper Part) and the Dioxomolybdenum Complexes $LMoO_2X$ (X = Cl, SCH_2Ph, OPh) (Lower Part)

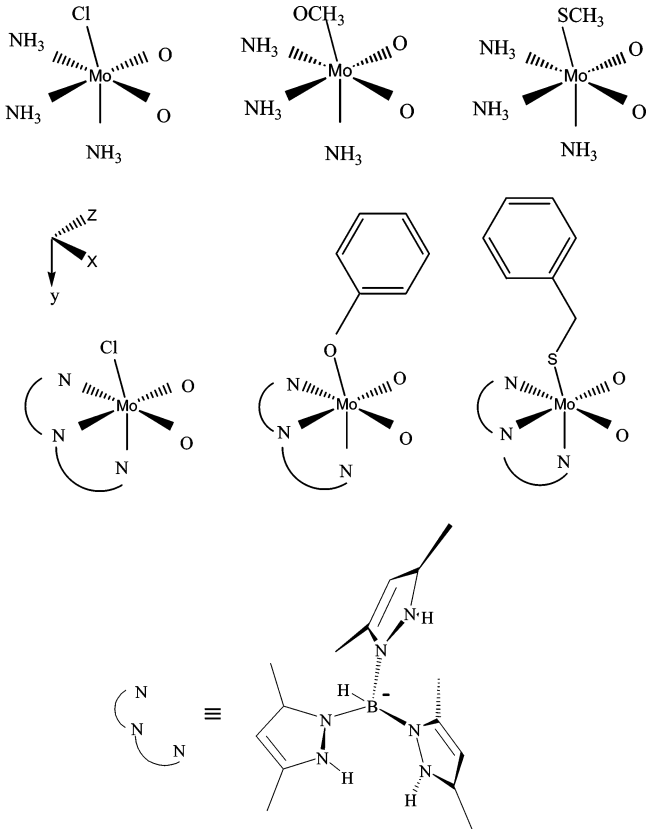

the range of the crystal distances reported in the literature[5] for dioxo-Mo complexes with slightly different tridentate N-donor ligands. The calculated Mo−N distances are 2.19, 2.17, and 2.20 Å for X = Cl, SCH_2Ph, and OPh, respectively.

All of the calculated spectra at the ligand 1s edge and Mo 2p edge have been convoluted with Gaussian functions with fwhm's of 1.3 and 1.8 eV, respectively, to facilitate the comparison with the experimental spectra.

4. Results and Discussion

The experimental spectra of the $LMoO_2X$ complexes[4] are analyzed in detail in the lowest-energy pre-edge region; therefore, we report in figures and tables the calculated excitation energies and oscillator strengths relative to the same energy range, both for the model molecules $[(NH_3)_3MoO_2X]^+$ and the $LMoO_2X$ complexes. This pre-edge region involves the electronic transitions toward the lowest virtual valence orbitals, which are mostly characterized by the 4d metal contribution with only small *n*p ligand participation. The intensity of these transitions maps the two different final orbital contributions through the excitations from the L metal and K ligand edges. Therefore, for a more complete discussion, it has appeared convenient to collect in a single table the results obtained for both edges of each compound.

4.1. Minimum Model Molecules. In the model molecules, the nitrogen atoms of the L ligand are replaced by three ammonia molecules, and the benzylthiolate and phenoxo ligands are substituted with SCH_3 and OCH_3 moieties, respectively. The coordinate system of the $[(NH_3)_3MoO_2X]^+$ (X = Cl, SCH_3, OCH_3) model used for the DFT calculations is presented in Chart 1. To correlate the calculated spectral features to the electronic structures of the model molecules, it can be useful to consider the MO scheme of the lowest virtual valence levels, which are characterized by strong 4d metal contribution, as already stressed (Figure 1). The splitting of the five 4d MOs can be interpreted as derived from a Mo esa-coordinated complex with a highly distorted O_h geometry. For each molecule, we observe a group of three MOs at lower energy (d_{xy}, d_{yz}, and d_{xz}), formally derived from the t_{2g} set in O_h symmetry, while the two MOs derived from the e_g set (d_{z^2} and $d_{x^2-y^2}$), are destabilized. The d_{z^2} MO has the highest energy in all molecules because of its strong antibonding interaction with the oxo groups, while the d_{xy} and d_{yz} MOs, which are diagonal with respect to the ligand's position, are the most stabilized.

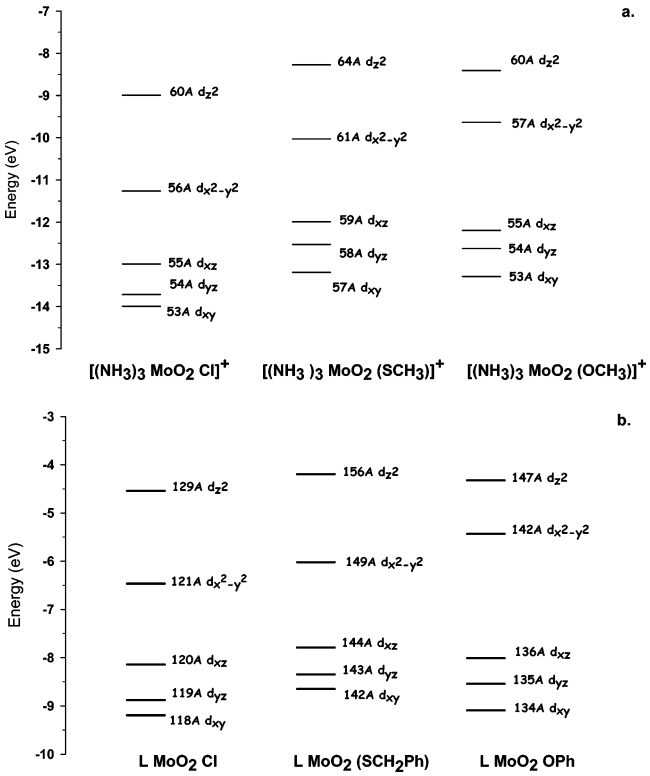

Figure 1. Energy diagram of the Mo 4d orbitals for the DFT ground state. Upper panel: $[(NH_3)_3MoO_2Cl]^+$, $[(NH_3)_3MoO_2SCH_3]^+$, and $[(NH_3)_3MoO_2OCH_3]^+$. Lower panel: $LMoO_2Cl$, $LMoO_2SCH_2Ph$, and $LMoO_2OPh$. The energy separations between the orbital energies are given in eV.

Ligand K Edge. The TDDFT Cl 1s and S 1s pre-edge excitation spectra of $[(NH_3)_3MoO_2Cl]^+$ and $[(NH_3)_3MoO_2SCH_3]^+$ are reported in Figure 2 and in Tables 1 and 2. The spectral features are associated with transitions from the ligand (Cl or S) 1s orbital, which has an essentially atomic character, and therefore, the dipole-allowed transitions gain intensity only if the final low-lying unoccupied MOs, generally dominated by the 4d metal character, also contain some 3p ligand contribution. This is likely to be small because the 3p AOs (of Cl or S atoms) also contribute to occupied orbitals; therefore, the relatively low values calculated for the pre-edge 1s features are not surprising.

The low-energy Cl 1s spectrum of $[(NH_3)_3MoO_2Cl]^+$ (Figure 2 and Table 1) exhibits two main structures separated by about 2.7 eV and followed by a small tail at higher energy. The first peak derives from the Cl 1s excitations into the first three lower MOs (53a, 54a, and 55a), which have a predominant 4d character (d_{xy}, d_{yz}, and d_{xz}, respectively). The highest intensity of the first transition toward the LUMO maps the larger

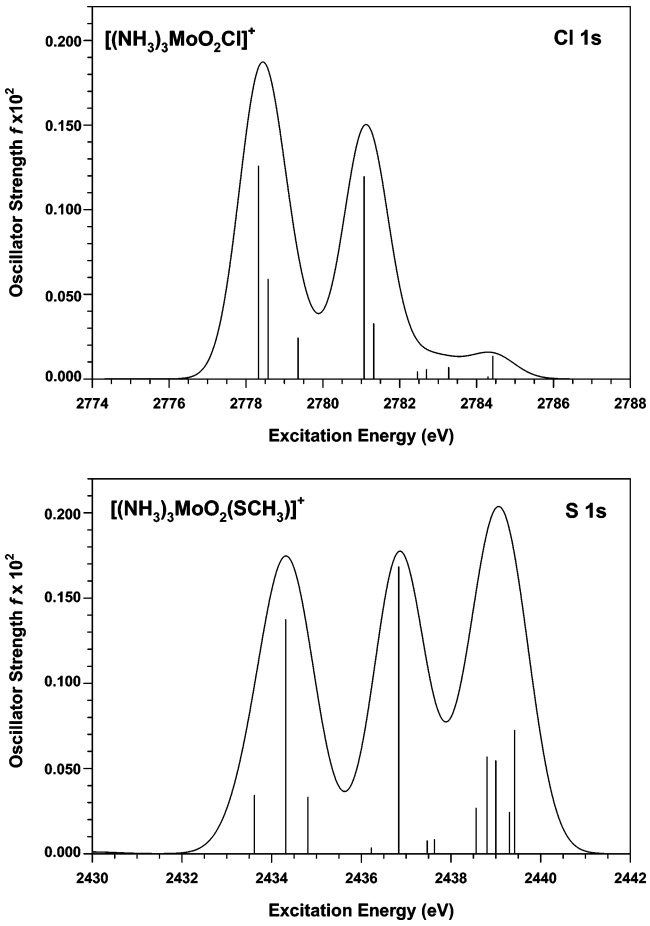

Figure 2. TDDFT Cl 1s and S 1s pre-edge excitation spectra of $[(NH_3)_3MoO_2Cl]^+$and $[(NH_3)_3MoO_2SCH_3]^+$. Calculated lines are convoluted with Gaussians of 1.3 eV fwhm.

contribution of the Cl 3p component in the 53a final state with respect to the next two MOs (54a and 55a), whose oscillator strengths decrease proportionally to their Cl 3p component (see Table 1). The second structure is contributed by two transitions toward the 56a and 57a MOs: The first one (at 2781.07 eV) is associated with the Cl 3p component of the $d_{x^2-y^2}$ level (56a), and its intensity is comparable to that calculated for the 53a transition, reflecting the similar Cl 3p participation in these final states. The small Cl 3p component in the 57a final state is responsible for the intensity drop of the relative line at 2781.32 eV. It is interesting to note that this final state has only a low 4d metal contribution, while the highest MO with strong 4d character (d_{z^2}) corresponds to the 60a final state. Here, the Cl 3p component is negligible and the intensity of the relative transition very low, as for the following lines which contribute to the small tail in the higher-energy part of the spectrum.

This analysis allows us to correlate the spectral features to the covalent bonding between the metal and the Cl ligand; the dominant contribution to the metal−ligand covalency is provided by the Cl 3pπ* and Cl 3pσ* (π and σ refer to the Mo−Cl bond) orbitals which significantly overlap with the Mo $4d_{xy}$ and $4d_{x^2-y^2}$ orbitals in the 53a and 56a levels, as probed by the higher intensity of the relative Cl 1s transitions in the spectrum. The interaction of the second Cl 3pπ* orbital with the $4d_{yz}$ orbital (in the 54a level) is instead weaker because of the tilt of the Mo−Cl bond in the direction opposite to the O−Mo−O diagonal, with a consequent reduction of the orbital overlap in accord with the decrease of the spectral intensity of the relative Cl 1s transition.

Consider now the results for $[(NH_3)_3MoO_2(SCH_3)]^+$ (Figure 2 and Table 2). Note that the shape of the S 1s spectrum appears different from the Cl 1s spectrum, with three bands of comparable intensity: The first one is assigned as transitions to the lowest virtual orbitals with mainly 4d character, the second is contributed by a single transition toward the 61a MO ($4d_{x^2-y^2}$), while the third and most intense band derives from many lines that are close in energy and of significant intensity. As concerns the first structure, the main difference with the X = Cl ligand is the shift of the intensity from the LUMO transition (57a) to the (LUMO + 1) transition (58a, at 2434.32 eV), which maps the higher S 3p participation in the 58a final orbital with respect to the 57a and 59a orbitals (see Table 2). This indicates that the thiolate π* orbital (S $3p_z$) overlaps principally with the $4d_{yz}$ orbital, in contrast to X = Cl, being the second S π* orbital ($3p_x$) involved in the S−C bonding and therefore not available for significant interaction with the lowest $4d_{xy}$ metal orbital. The third S 3p orbital ($3p_y$) can interact primarily with the $4d_{x^2-y^2}$ orbital, to give rise to a σ* orbital, which corresponds to the final state (61a) of the S 1s transition at 2436.84 eV and is responsible for the second strong peak of the spectrum. This shows that the dominant contribution to the metal−ligand covalency comes from the interaction between the S 3pσ* and $4d_{x^2-y^2}$ orbitals, as found also in the case of the Cl ligand. The first two peaks are separated by about 2.5 eV, a value very close to that found for the X = Cl compound, therefore suggesting a similar splitting between the first three metal d orbitals and the $d_{x^2-y^2}$ orbital in the two model molecules, as confirmed also by the energetic scheme of Figure 1. The higher-energy transitions which give rise to the third spectral feature sample the S 3p content of the higher virtual MOs. The oscillator strength distribution also reflects a certain mixing among 1h−1p configurations, in particular in the 67a and 68a final states. The S 3p content represents the virtual counterpart of the S $3p_x$ orbital involved in the S−C bond, which is pushed to higher-lying virtual MOs and is responsible for the different spectral response to the bonding situation with respect to the X = Cl ligand. It has to be noted that the highest 4d metal orbital, d_{z^2}, contributes to the 64a virtual orbital, whose S 3p component is quite small, as is apparent from the low intensity calculated for the corresponding transition.

The results obtained for the ligand K edge show that there is a proportionality between the calculated intensity of the ligand features and the mixing of ligand orbitals into the metal d orbitals, confirming the capability of the XAS ligand spectra to probe the covalency of the metal−ligand bond.

Molybdenum L Edge. Consider now the 2p metal edge: The relative excitations are expected to be dominated by the 2p−4d transition moment, which directly probes the molybdenum 4d content of the different unoccupied levels and, therefore, the details of the d involvement into the bonding. The results are reported in Figure 3 and in Tables 1−3. The complexity of the spectra, with respect to the ligand K edge, derives from the large number of lines which contribute to the calculated features, as is apparent in Figure 3. Because of the lack of symmetry elements in these molecules, for each final orbital, there are three distinct transitions starting from the three Mo 2p orbitals, whose SCF energies are slightly different; furthermore, the effect of the 1h−1p configuration mixing included in the TDDFT calculations can further split the relative excitation energies. The theoretical spectra of $[(NH_3)_3MoO_2Cl]^+$ and $[(NH_3)_3MoO_2(SCH_3)]^+$ exhibit three main features: a lower-energy and most-intense peak followed by a middle, less-resolved structure, and then a last, higher-energy peak. The second and third peaks

TABLE 1: Calculated TDDFT Excitation Energies (*E*(eV)) and Oscillator Strengths (*f*) for Chlorine 1s and Molybdenum 2p Excitation Spectra of $[(NH_3)_3MoO_2Cl]^+$ [a]

Cl 1s		final		Mo 2p		configuration mixing
E (eV)	$f \times 10^2$	state	Mo 4d and Cl 3p character	*E* (eV)	$f \times 10^2$	in Mo 2p transitions
2778.33	0.126	53a	Mo $4d_{xy}$ (57%) + Cl 3p (12%)	2499.93	0.001	53a
				2500.06	0.095	53a + 54a
				2500.15	0.364	53a
2778.58	0.059	54a	Mo $4d_{yz}$ (56%) + Cl 3p (6%)	2500.22	0.002	54a
				2500.44	0.379	54a
				2500.56	0.880	54a + 53a
2779.35	0.024	55a	Mo $4d_{xz}$ (55%) + Cl 3p (2%)	2500.09	0.316	55a
				2501.18	0.487	55a
				2501.44	1.225	55a
2781.07	0.120	56a	Mo $4d_{x^2-y^2}$(41%) + Cl 3p (10%)	2502.68	0.043	56a
				2502.78	0.308	56a + 57a
				2502.85	0.119	56a + 57a
2781.32	0.033	57a	Mo $4d_{x^2-y^2}$ (10%) + Cl 3p (1.5%)	2502.95	0.010	57a
				2503.04	0.491	57a + 56a
				2503.23	1.025	57a + 56a
2782.46	0.004	58a	H 1s + N 2p	2504.09	0.004	58a
				2504.10	0.026	
				2504.11	0.017	
2782.70	0.005	59a	H 1s + N 2p	2504.32	0.004	59a
				2504.33	0.013	
				2504.34	0.043	
2783.28	0.006	60a	Mo $4d_{z^2}$ (47%)	2504.95	~0	60a
				2505.25	0.921	
				2505.31	0.820	
2783.85	0.0003	61a	Mo $4d_{xy}$ (4%)	2505.48	0.018	61a
				2505.49	0.044	
				2505.50	0.078	
2784.29	0.001	62a	Mo $4d_{x^2-y^2}$ (3%)	2505.92	0.012	62a
				2505.93	0.010	
				2505.93	0.030	

[a] Calculated Cl 1s and Mo 2p DFT-KS eigenvalues (ionization thresholds) are 2792.26 and 2513.89 eV, respectively.

coalesce into only one peak in the $[(NH_3)_3MoO_2OCH_3]^+$ spectrum, reflecting the different energy splitting of the transition lines which distribute into two distinct groups, which is apparent as well in Figure 3. The spectral behavior can be rationalized by considering the diagram of the virtual valence levels with mainly Mo 4d character, reported in Figure 1. In the Cl complex, the five 4d levels are split into three groups by the ligand field: the lower-lying d_{xy}, d_{yz}, and d_{xz} MOs which are close in energy, then the $d_{x^2-y^2}$ orbital which lies at approximately 2 eV from both the lowest MO group, and the highest d_{z^2} orbital. The splitting of the 4d orbitals is consistent with the shape of the calculated spectrum in Figure 3: The first peak (at about 2500.4 eV) is relative to the transitions toward the lowest 4d orbitals (53a, 54a, and 55a). The mixing among the 1h−1p configurations in the 53a and 54a final states is responsible for a nonequivalent intensity distribution between the two states, as expected on the grounds of their similar 4d content (see Table 1). The middle peak (around 2503 eV) is associated with the Mo 2p transitions to the $4d_{x^2-y^2}$ component present in the 56a and 57a final states. Also in this case, the intensity distribution between these two final states does not reflect the 4d participation to the MOs (41% in 56a and 10% in 57a) but, rather, reflects the mixing of the 2p → 56a and 2p → 57a excitations in the final states as reported in Table 1. The last calculated peak is attributed to the excitations to the higher-lying $4d_{z^2}$ final orbital, which characterizes the 60a final state at approximately 2505 eV.

The three-peaked shape is maintained also in the thiolate spectrum according to the similar energy splitting of the Mo 4d orbitals, as shown in Figure 1. The first peak (around 2500 eV) is assigned to the transitions toward the lower-lying 4d orbitals (57a, 58a, and 59a), and its intensity is comparable to that calculated for the Cl complex. The middle peak is essentially associated with the 2p → 61a ($4d_{x^2-y^2}$) transitions around 2502.7 eV; it is characterized by smaller intensity with respect to that obtained for the corresponding peak of the previous molecule and a reversed shape for the presence of a higher-energy tail associated with the small $4d_{x^2-y^2}$ component present in the 63a final state. The most significant difference with the Cl complex spectrum is relative to the third peak, which appears to be contributed by several transitions of comparable intensity in SCH_3. Although we can identify the 64a final orbital as mainly 4d (d_{z^2}) in character (about 37%), we do not calculate significant oscillator strength for the 2p transition toward this MO; instead, the intensity is spread over other excited states with less significant 4d metal participation. This is an effect of the strong mixing of 1h−1p configurations (2p → 64a, 2p → 65a, and 2p → 66a) in the final states lying in the 2504−2505 eV energy range.

The spectrum of the alkoxide complex (Figure 3 and Table 3) shows only two features of similar intensity. The first one manifests the same nature as in the two previous compounds, derived from the transitions to the lowest 4d MOs of the alkoxide. Also, the energy range covered by these transitions is similar to that of the other two compounds (the peak is centered at 2500.8 eV), as well as the intensity. The strongest difference is the disappearance of the middle peak in the spectrum: This is an effect of different splitting of the metal d orbitals, as is apparent in Figure 1. We observe an increase of the energy separation between the lower-lying 4d orbitals and the most destabilized $d_{x^2-y^2}$ and d_{z^2} orbitals (in the alkoxide, this splitting is approximately 2.6 eV, while it is approximately 1.8 and 2 eV in X = Cl and X = SCH_3 complexes, respectively) and a parallel decrease of the splitting between the last two d levels. This is responsible for the energy positions of the relative transitions and the appearance of only one higher-energy peak in the spectrum. This peak is centered at approximately 2505 eV and derives from several transitions toward final states with

TABLE 2: Calculated TDDFT Excitation Energies (*E*(eV)) and Oscillator Strengths (*f*) for Sulfur 1s and Molybdenum 2p Excitation Spectra of $[(NH_3)_3MoO_2(SCH_3)]^+$ [a]

S 1s		final		Mo 2p		configuration mixing
E (eV)	$f \times 10^2$	state	Mo 4d and S 3p character	*E* (eV)	$f \times 10^2$	in Mo 2p transitions
2433.61	0.034	57a	Mo $4d_{xy}$ (58%) + S 3p (4%)	2499.44	0.003	57a
				2499.63	0.383	
				2499.65	0.282	
2434.32	0.137	58a	Mo $4d_{yz}$ (50%) + S 3p (16%)	2500.13	0.0004	58a
				2500.29	0.261	58a
				2500.38	0.607	58a + 59a
2434.81	0.033	59a	Mo $4d_{xz}$ (54%) + S 3p (4%)	2500.71	0.369	59a
				2500.85	0.619	
				2501.07	1.093	
2436.22	0.003	60a	H 1s + Mo 5s	2502.02	0.004	60a
				2502.03	0.003	
				2502.05	0.009	
2436.84	0.168	61a	Mo $4d_{x^2-y^2}$ (43%) + S 3p (20%)	2502.64	0.028	61a
				2502.78	0.583	
				2502.92	0.668	
2437.47	0.008	62a	H 1s + N 2p	2503.28	0.016	62a
				2503.29	0.028	
				2503.30	0.007	
2437.63	0.008	63a	Mo $4d_{x^2-y^2}$ (3%) + S 3p (2%)	2503.44	0.032	63a
				2503.46	0.062	
				2503.50	0.290	
2438.56	0.027	64a	Mo $4d_{z^2}$ (37%) + S 3p (7%)	2504.38	0.010	64a
				2504.49	0.080	64a + 65a
				2504.52	0.151	64a + 65a
2438.80	0.057	65a	Mo $4d_{z^2}$ (11%) + S 3p (20%)	2504.60	0.059	65a
				2504.71	0.318	65a + 66a
				2504.74	0.225	65a + 66a
2439.00	0.055	66a	Mo $4d_{z^2}$ (5%) + S 3p (8%)	2504.78	0.005	66a
				2504.84	0.276	66a
				2504.87	0.368	66a + 65a
2439.30	0.024	67a	Mo $4d_{z^2}$ (3%) + S 3p (6%)	2505.09	0.022	67a
				2505.11	0.056	67a
				2505.16	0.149	67a + 68a
2439.42	0.072	68a	Mo $4d_{z^2}$ (2%) + S 3p (7%)	2505.18	0.010	68a
				2505.24	0.224	68a
				2505.25	0.372	68a + 67a

[a] Calculated S 1s and Mo 2p DFT-KS eigenvalues (ionization thresholds) are 2446.83 and 2512.64 eV, respectively.

different $d_{x^2-y^2}$ and d_{z^2} metal contribution and different intensities. As we can see in Table 3, the 2p → $4d_{x^2-y^2}$ transition involves the 57a and 59a final states (at 2503.8 and 2504.2 eV) which are mixed by the 1h−1p configuration interaction with a consequent redistribution of the intensity, which concentrates on the final state at 2504.3 eV. A quite large oscillator strength is calculated for the 2p → 60a transition which reflects the significant d_{z^2} contribution to the 60a final orbital; the lower-intensity lines at higher energy derive from transitions toward final states, among which the d_{z^2} content redistributes with lower weight.

4.2. Dioxomolybdenum Complexes. The energy diagram of the virtual MOs containing strong Mo 4d contribution (Figure 1) can be used as a guide for the interpretation of the calculated XAS spectra of the $LMoO_2X$ (X = Cl, SCH_2Ph, OPh) complexes. The coordinate systems used for the DFT calculations are shown in Chart 1. As we can see, all three molecules show the same ordering of the Mo 4d MOs: a group of three low-lying orbitals, which have the energy order $d_{xy} < d_{yz} < d_{xz}$ and are well separated by the two most destabilized $d_{x^2-y^2}$ and d_{z^2} orbitals, with the energy of d_{z^2} greater than that of $d_{x^2-y^2}$. We can note that the calculated 4d energy splitting for the complexes is analogous to that found for the model molecules.

Ligand K Edge. The TDDFT-calculated Cl and S K edge spectra of $LMoO_2(SCH_2Ph)$ and $LMoO_2(OPh)$ are reported in Tables 4 and 5 and in Figure 4 together with the experimental profiles.[4]

The theoretical Cl 1s spectrum shows two main features centered at 2778.9 and 2781.6 eV and reproduces correctly the experimental pattern (Figure 4). The main discrepancy is the strong underestimate of the calculated excitation energies with respect to the experimental results (see caption to Figure 4), a typical problem ascribed to the self-interaction present in DFT, which is particularly important for core excitations. However, for the discussion of the spectra, it is more important to consider the energy splitting between the features than the absolute scale; therefore, to facilitate the comparison, we have shifted the experimental spectrum on the calculated energy scale. We can note the nice reproduction of the energy separation between the two first peaks, which amounts to 2.7 eV in the calculation and 2.3 eV in the experiment, while the intensity of the second structure appears to be underestimated in the calculation, producing a reversed intensity trend with respect to the experiment. The first peak is assigned to the Cl 1s transitions toward the three lower-lying virtual orbitals (118a, 119a, and 120a in Table 4) with predominant Mo 4d character ($4d_{xy}$, $4d_{yz}$, and $4d_{xz}$, respectively) and only a small contribution from the Cl ligand. This is highest for the LUMO (Cl 3pπ component) and decreases for the next two MOs, as correctly mapped by the calculated oscillator strengths. The second peak corresponds to the transitions toward the three following final states (121a, 122a, and 123a) characterized by different $4d_{x^2-y^2}$ contributions and by smaller Cl 3p components. The similar intensity calculated for these lines does not reflect the different Cl 3p contributions to the final states (Table 4) and depends on the slight mixing of the Cl 1s → 121a and Cl 1s → 122a configurations, which redistributes the oscillator strengths over the final states. It has to be noted that the highest MO with 4d metal character ($4d_{z^2}$), corresponding to the 129a final state, has only a negligible Cl 3p participation and does not contribute to

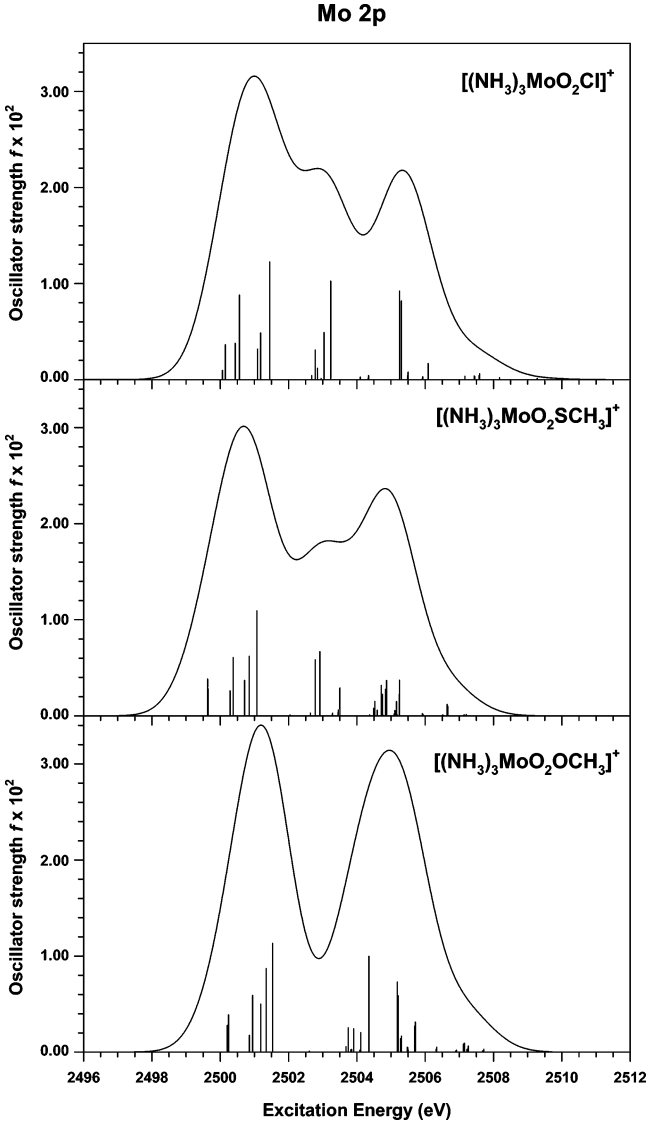

Figure 3. TDDFT Mo 2p pre-edge excitation spectra of $[(NH_3)_3MoO_2Cl]^+$, $[(NH_3)_3MoO_2SCH_3]^+$, and $[(NH_3)_3MoO_2OCH_3]^+$. Calculated lines are convoluted with Gaussians of 1.8 eV fwhm.

any spectral feature. The higher-energy tail in the calculated spectrum, not considered in the experiment, derives from transitions to virtual MOs with ligand contributions. Apart from fine details, the interpretation of the two pre-edge features is analogous to that proposed for the corresponding model molecule as well as the considerations made for the covalent bonding between the Mo and Cl ligands: The most significant overlap is realized between the Cl 3pπ* and Mo 4d_{xy} and between Cl 3pσ* and Mo 4$d_{x^2-y^2}$ orbitals.

The theoretical results for the S 1s spectrum of $LMoO_2(SCH_2Ph)$ are reported in Table 5 and Figure 4, where the experimental data are also shown (shifted on the calculated energy scale). The reported experimental features have been obtained through a background subtraction from the normalized spectrum;[4] this procedure has ruled out the intensity contribution from structures lying at higher energies. For this reason, we have chosen to compare our theoretical results with the difference spectrum of ref 4 and to limit the discussion only to the two lower-energy features. As we can see, the agreement between theory and experiment is very satisfactory, both concerning the energy separation of the first two peaks (2.3 eV in the calculation and 2.0 eV in the experiment) and the intensity distribution. The first peak is contributed by three transitions to the lowest 4d

TABLE 3: Calculated TDDFT Excitation Energies (*E*(eV)) and Oscillator Strengths (*f*) for Molybdenum 2p Excitation Spectrum of $[(NH_3)_3MoO_2(OCH_3)]^+$ [a]

E (eV)	$f \times 10^2$	final state	Mo 4d and O 2p character[b]	configuration mixing
2499.98	0.002	53a	Mo 4d_{xy} (62%)+ O 2p (3%)	53a
2500.21	0.278			
2500.24	0.388			
2500.67	0.0005	54a	Mo 4d_{yz} (57%)+ O 2p (9%)	54a
2500.85	0.176			54a + 55a
2500.95	0.591			54a + 55a
2501.19	0.500	55a	Mo 4d_{xz} (54%) + O 2p (1%)	55a + 54a
2501.34	0.869			55a + 54a
2501.53	1.132			55a
2502.57	0.006	56a	H 1s + Mo s	56a
2502.59	0.009			
2502.61	0.010			
2503.68	0.057	57a	Mo 4$d_{x^2-y^2}$ (41%) + O 2p (7%)	57a
2503.75	0.254			57a
2503.90	0.243			57a + 59a
2503.82	0.023	58a	H 1s + N 2p	58a
2503.84	0.028			
2503.85	0.029			
2504.09	0.021	59a	Mo 4$d_{x^2-y^2}$ (11%)	59a
2504.11	0.204			59a
2504.35	0.999			59a + 57a
2504.90	0.010	60a	Mo 4d_{z^2} (47%)	60a
2505.18	0.730			
2505.21	0.587			
2505.28	0.141	61a	Mo 4d_{xy} (5%)	61a
2505.30	0.076			
2505.31	0.166			
2505.47	0.051	62a	Mo 4$d_{x^2-y^2}$ (2%)	62a
2505.49	0.046			
2505.50	0.023			
2505.67	0.005	63a	Mo 4d_{z^2} (4%)	63a
2505.69	0.270			
2505.71	0.313			

[a] Calculated Mo 2p DFT-KS eigenvalue (ionization threshold) is 2513.3 eV. [b] The O 2p contribution to the final state is relative to the oxygen atom of the alkoxide ligand.

virtual orbitals (142a, 143a, and 144a) with the highest intensity associated with the LUMO + 1 orbital (4d_{yz}), which has the most significant overlap with the S 3pπ* component (see Table 5). The second band centered at 2436.79 eV is assigned to the 149a transition, whose high intensity reflects the significant S 3p contribution (S 3pσ*) to the final orbital dominated by the 4$d_{x^2-y^2}$ component. The last and most intense calculated structure is mostly contributed by the transition to the 155a final state, which is characterized by a strong S 3p participation and only a minor 4d_{z^2} contribution. The 4d_{z^2} component characterizes the 156a MO whose S 3p content is, however, negligible. It is interesting to notice that our calculated S 1s ionization threshold (2442.77 eV, see Table 5) lies more than 8 eV above the first calculated structure. This suggests that the background subtraction performed on the experimental data might be revised with a shift to higher energies, to ascribe a wider energy range to the pre-edge region. In summary, the calculated S 1s spectral behavior for the $LMoO_2(SCH_2Ph)$ complex closely resembles that obtained for its model analogues, also concerning the main differences with the X = Cl complex. This behavior can be related to the similarity of the calculated 4d orbital energy splitting for the models and the $LMoO_2X$ molecules and of the extent of mixing between 4d metal and S 3p ligand components in the lower-lying virtual MOs.

Molybdenum L Edge. The TDDFT results for the Mo L edge spectra of $LMoO_2Cl$, $LMoO_2(SCH_2Ph)$, and $LMoO_2(OPh)$ are reported in Tables 4, 5, and 6 and in Figure 5 together with the experimental profiles relative to the L_3 edge spectra. These are

TABLE 4: Calculated TDDFT Excitation Energies (*E*(eV)) and Oscillator Strengths (*f*) for Chlorine 1s and Molybdenum 2p Excitation Spectra of $[LMoO_2Cl]^+$ [a]

Cl 1s		Mo 2p		final		configurations mixing
E (eV)	$f \times 10^2$	*E* (eV)	$f \times 10^2$	state	Mo 4d and Cl 3p character	in Mo 2p transition
2778.74	0.1079	2499.99	0.001	118a	Mo $4d_{xy}$ (56%) + Cl 3p (10%)	118a
		2500.13	0.115			118a + 119a
		2500.21	0.357			118a
2779.04	0.0603	2500.31	~0	119a	Mo $4d_{yz}$ (55%) + Cl 3p (6%)	119a
		2500.53	0.348			119a
		2500.65	0.823			119a + 118a
2779.76	0.0180	2501.13	0.309	120a	Mo $4d_{xz}$ (55%) + Cl 3p (<1%)	120a
		2501.23	0.507			120a
		2501.47	1.157			120a
2781.46	0.0363	2502.72	0.032	121a	Mo $4d_{x^2-y^2}$ (31%) + Cl 3p (7%)	121a
		2502.75	0.042			121a + 122a
		2502.77	0.009			122a + 121a
2781.53	0.0417	2502.79	0.056	122a	Mo $4d_{x^2-y^2}$ (8%) + Cl 3p (2%)	122a
		2502.81	0.070			122a + 123a + 121a
		2502.86	0.054			123a + 121a + 122a
2781.65	0.0488	2502.91	0.001	123a	Mo $4d_{x^2-y^2}$ (13%) + Cl 3p (2%)	123a
		2503.06	0.652			123a + 121a
		2503.29	1.173			123a + 121a + 122a
2782.17	0.0030	2503.43	0.0004	124a	ligand orbitals	124a
		2503.44	0.005			
		2503.45	0.053			
2782.76	0.0002	2504.03	0.002	125a	ligand orbitals	125a
		2504.03	0.011			
		2504.04	0.004			
2783.31	0.002	2504.58	0.004	128a	Mo $4d_{z^2}$ (7%)	128a + 129a
		2504.59	~0			128a
2783.35	0.0013	2504.66	~0	129a	Mo $4d_{z^2}$ (41%) + O 2p (20%)	129a
		2504.98	1.065			129a + 128a
		2505.03	0.961			129a + 128a

[a] Calculated Cl 1s and Mo 2p DFT-KS eigenvalues (ionization thresholds) are 2787.89 and 2509.16 eV, respectively.

TABLE 5: Calculated TDDFT Excitation Energies (*E*(eV)) and Oscillator Strengths (*f*) for Sulfur 1s and Molybdenum 2p Excitation Spectra of $[LMoO_2(SCH_2Ph)]^+$ [a]

S 1s		Mo 2p		final		configuration mixing
E (eV)	$f \times 10^2$	*E* (eV)	$f \times 10^2$	state	Mo 4d and S 3p character	in Mo 2p transitions
2434.15	0.0493	2499.83	0.003	142a	Mo $4d_{xy}$ (57%) + S 3p (5%)	142a
		2499.97	0.132			142a + 143a
		2500.02	0.283			142a
2434.47	0.1174	2500.15	0.015	143a	Mo $4d_{yz}$ (49%) + S 3p (12%)	143a
		2500.30	0.275			143a
		2500.44	0.649			143a + 142a
2435.00	0.0314	2500.77	0.392	144a	Mo $4d_{xz}$ (54%) + S 3p (3%)	144a
		2500.88	0.510			
		2501.12	1.151			
2436.39	0.0162	2502.07	0.008	145a	Mo $4d_{mixed}$ (11%) + S 3p (3%)	145a
		2502.09	0.053			
		2502.10	0.048			
2436.48	0.0015	2502.16	0.011	146a	Mo $4d_{yz}$ (1%)	146a
		2502.17	0.028			
		2502.18	0.030			
2436.56	0.0154	2502.22	0.005	147a	S 3p (1%)	147a
		2502.23	0.006			
		2502.24	0.004			
2436.62	0.0028	2502.29	0.015	148a	ligand orbitals	148a
		2502.30	0.017			
		2502.31	0.022			
2436.82	0.1449	2502.48	0.013	149a	Mo $4d_{x^2-y^2}$ (34%) + S 3p (16%)	149a
		2502.63	0.621			149a
		2502.75	0.616			149a + 150a
2437.17	0.0058	2502.84	0.023	150a	ligand orbitals	150a
		2502.86	0.035			150a
		2502.87	0.278			150a + 149a
2438.50	0.1774	2504.08	0.011	155a	Mo $4d_{z^2}$ (3%) + S 3p (36%)	155a
		2504.09	0.009			
		2504.12	0.139			
2438.58	0.0023	2504.28	0.004	156a	Mo $4d_{z^2}$ (43%)	156a
		2504.51	0.368			156a + 158a
		2504.53	0.218			156a + 158a
2438.79	0.0490	2504.44	0.002	157a	S 3p (3%)	157a
2438.89	0.0120	2504.56	0.0121	158a	ligand orbitals	158a
		2504.58	0.0939			158a + 156a
		2504.61	0.1385			158a + 156a

[a] Calculated S 1s and Mo 2p DFT-KS eigenvalues (ionization thresholds) are 2442.77 and 2508.45 eV, respectively.

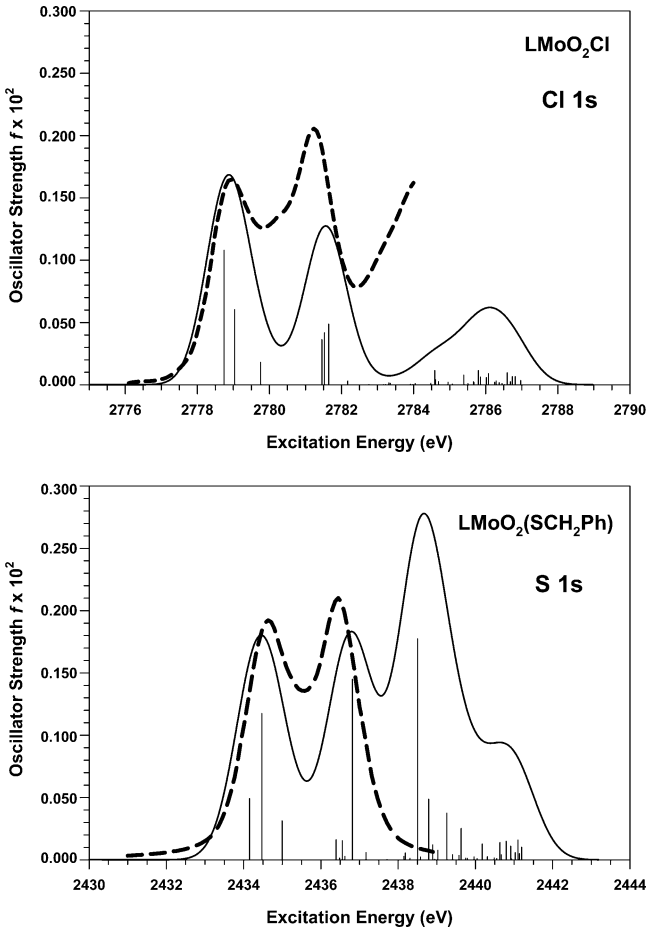

Figure 4. Cl 1s and S 1s pre-edge excitation spectra of $LMoO_2Cl$ and $LMoO_2SCH_2Ph$. Solid line: TDDFT results. Dashed line: experimental data from ref 4. The experimental features have been shifted on the calculated energy scale. The energies of the two experimental features are 2821.9 and 2824.2 eV for $LMoO_2Cl$ and 2470.5 and 2472.5 eV for $LMoO_2SCH_2Ph$.

shifted to the calculated energy scale in order to facilitate the comparison between the spectral trends. It should be noted that the present nonrelativistic TDDFT scheme does not allow the explicit treatment of the spin−orbit effect, and therefore, it is not possible to distinguish between the L_2 and L_3 edges. For 4d systems, differences in spectral shape between the L_2 and L_3 edges have been experimentally observed, in particular for Mo compounds,[25,26] and have been associated principally to the multiplet effects consisting of coupling the 2p core wave function to the valence states of 4d character with only a minor contribution from the spin−orbit coupling.[27] Furthermore, the L_2 edge of 4d systems is less affected by multiplet effects than the L_3 edge.[26] Because of the capability of the TDDFT scheme to include these effects, we have chosen to compare our results with the L_3 experimental spectra, although in the work of Izumi et al.,[4] the analysis of the experimental data has been focused on the L_2 edge features.

The calculated splitting of the Mo 4d orbitals for the complexes, reported in Figure 1, shows a similar trend for the Cl and SCH_2Ph ligands with a grouping of the orbitals in three sets: the lower-lying corresponding to the $4d_{xy}$, $4d_{yz}$, and $4d_{xz}$ orbitals, then the intermediate $4d_{x^2-y^2}$ orbital, and last, the highest $4d_{z^2}$ orbital. In the OPh complex, the $4d_{x^2-y^2}$ orbital is more destabilized and close to the $4d_{z^2}$ orbital; therefore, the 4d orbitals appear grouped in two sets. This trend is analogous to that of the model molecules; therefore, we can also expect that the shapes of the Mo 2p spectra are maintained in the case of

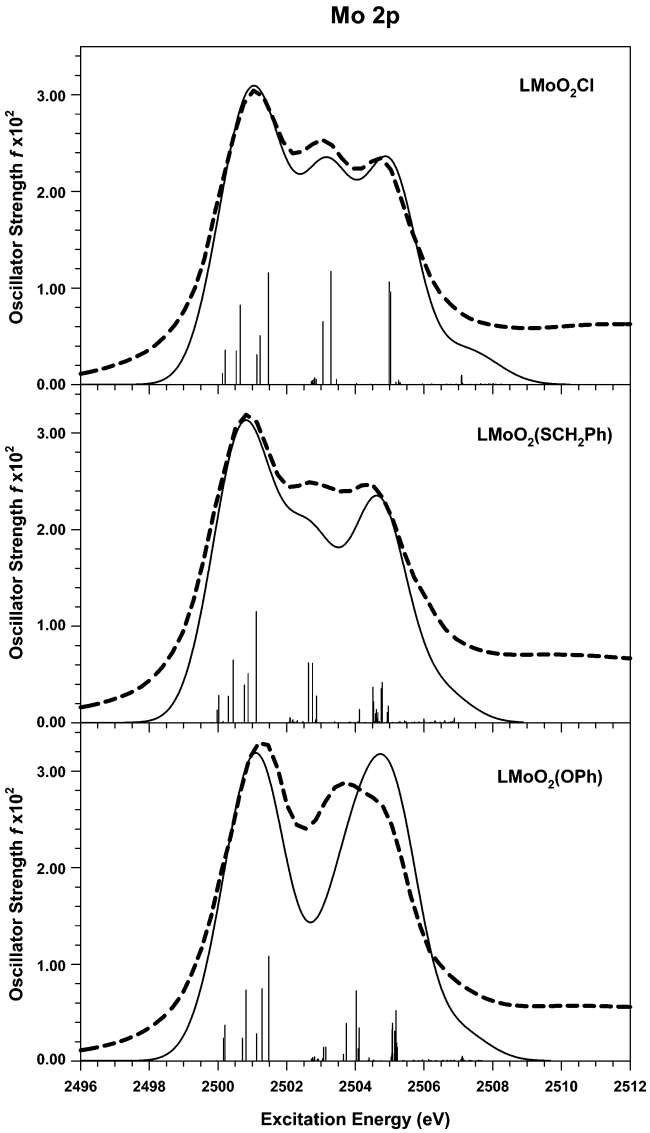

Figure 5. Mo 2p pre-edge excitation spectra of $LMoO_2Cl$, $LMoO_2SCH_2Ph$, and $LMoO_2OPh$. Solid line: TDDFT results. Dashed line: experimental data from ref 4. The experimental features have been shifted on the calculated energy scale.

the $LMoO_2X$ complexes. In detail, we observe that the TDDFT spectrum of $LMoO_2Cl$ has a strong peak around 2501 eV followed by two less-intense structures around 2503 and 2505 eV. The agreement with the experiment is very satisfactory, both concerning the energy separations among the peaks and the intensity distribution. The first peak is assigned as Mo 2p transitions to the $4d_{xy}$, $4d_{yz}$, and $4d_{xz}$ levels (118a, 119a, and 120a in Table 4), while the second peak is associated with the $2p \rightarrow 4d_{x^2-y^2}$ transition. The $4d_{x^2-y^2}$ contribution is present with different weights in three final states (121a, 122a, and 123a), which are also mixed by the configuration interactions with a consequent redistribution of the calculated oscillator strengths, as reported in Table 4. The last peak is assigned to the $4d_{z^2}$ transition which involves the two mixed final states 128a and 129a. This pattern is consistent with the calculated 4d splitting (Figure 1) as well as with the Mo 2p theoretical spectrum of the Cl model molecule.

A similar spectral shape is also calculated for the $LMoO_2(SCH_2Ph)$ complex, with only the middle peak appearing less resolved than in the Cl complex. Also, the attribution of the spectral features is analogous to that proposed for the Cl complex. The comparison with the experimental results is nice,

TABLE 6: Calculated TDDFT Excitation Energies (*E*(eV)) and Oscillator Strengths (*f*) for Molybdenum 2p Excitation Spectrum of $LMoO_2(OPh)$[a]

E (eV)	$f \times 10^2$	final state	Mo 4d and O 2p character	configuration mixing
2499.96	~0	134a	Mo $4d_{xy}$ (60%) + O 2p (1%)	134a
2500.16	0.2346			
2500.20	0.3704			
2500.53	~0	135a	Mo $4d_{yz}$ (52%) + O 2p (7%)	135a
2500.72	0.2352			
2500.82	0.7334			
2501.12	0.2820	136a	Mo $4d_{xz}$ (55%)	136a
2501.29	0.7469			
2501.47	1.0860			
2502.72	0.0211	137a	Mo $4d_{x^2-y^2}$ (3%)	137a
2502.74	0.0147			
2502.76	0.0360			
2502.88	0.0100	139a	Mo $4d_{x^2-y^2}$ (2%)	139a
2502.91	0.0187			
2502.92	0.0179			
2503.04	0.0237	140a	Mo $4d_{x^2-y^2}$ (14%) + O 2p (3%)	140a
2503.08	0.1414			
2503.13	0.1427			
2503.65	0.0685	142a	Mo $4d_{x^2-y^2}$ (37%) + O 2p (12%)	142a
2503.74	0.3875			142a
2504.03	0.7262			142a + 143a
2504.08	0.1256	143a	ligand orbitals	143a
2504.09	0.0500			143a
2504.11	0.3428			142a + 143a
2504.76	0.016	147a	Mo $4d_{z^2}$ (46%)	147a
2505.04	0.0402	148a	Mo *n*s (17%)	148a
2505.06	0.0755			148a
2505.067	0.3243			148a + 147a + 149a
2505.073	0.2372			148a + 147a
2505.08	0.3903			147a + 149a
2505.13	0.0679	149a	ligand orbital	149a
2505.15	0.3082			149a + 147a
2505.18	0.5214			149a + 147a

[a] Calculated Mo 2p DFT-KS eigenvalue (ionization threshold) is 2509.04 eV. [b] The O 2p contribution to the final state is relative to the oxygen atom of the phenoxo group.

apart from the slight underestimate of the intensity of the second band. This is due to a different distribution of the $4d_{x^2-y^2}$ component over the virtual levels, which concentrates with significant weight (34%) only in the 149a orbital with a consequent reduction of the oscillator strength calculated for the relative transition.

A different spectral pattern is instead calculated for the $LMoO_2(OPh)$ spectrum which shows only two structures of similar intensity, in good accord with the experiment apart from an overestimate of the energy separation of the two peaks. The first structure (around 2501 eV) has the same nature as in the previous complexes, and the oscillator strength is also comparable, as the 4d contribution to the involved final states of the same magnitude (around 50%) found in the other compounds. The coalescence of the second and third peaks is associated to the different splitting of the 4d orbitals in the OPh complex, as previously commented. The second band is at 2504.7 eV, therefore in the same energy region of the third band of the Cl and SCH_2Ph spectra, and is assigned to the transitions toward the $4d_{x^2-y^2}$ and $4d_{z^2}$ orbitals. This justifies the higher calculated intensity with respect to the third band in the other two spectra, also in line with the experimental observation. The calculations (Table 6) indicate that the intensity is distributed over two groups of lines: a first group relative to the final levels with $4d_{x^2-y^2}$ contribution (137a, 139a, 140a, and 142a), which covers the energy range between 2502.7 and 2504 eV, and a second group of the $2p \rightarrow 4d_{z^2}$ transitions, around 2505 eV, described by strongly mixed configurations which spread the oscillator strength over several lines very close in energy. In summary, the distribution of the oscillator strengths in the Mo 2p spectra probes the 4d metal content of the lowest-lying virtual levels; the spectral shape directly reflects the 4d orbital energy splitting and its variation along the series as an effect of the covalent contribution from the X ligand.

5. Conclusions

The TDDFT method extended to the treatment of the core electron excitations has been applied to the calculations of the XAS spectra at the Cl and S K edge and Mo L edge of a series of dioxomolybdenum complexes $LMoO_2X$ (X = Cl, SCH_2Ph, and OPh). The good agreement with the experimental data points out the reliability of the computational scheme for the description of excitation energies and oscillator strengths even in the case of a degenerate core hole (Mo 2p), where the proper mixing of configurations is a necessary condition to obtain reliable results. The relative computational economy of the present TDDFT method makes it a good candidate to treat the core excited states of large and low-symmetry molecules, such as bioinorganic systems, with reasonable effort and affordable predictions.

The study has also considered the simulation of the XAS spectra of the $[(NH_3)_3MoO_2X]^+$ (X = Cl, SCH_3, OCH_3) analogues, showing that these model molecules correctly mimic the spectral behavior of the dioxomolybdenum complexes, both at the K edge of the ligands and the L edge of the metal. The interpretation of the spectral features can be supported by the calculated 4d orbital energy splittings which are useful also to correlate the spectral trends along the series with the change of the X ligand, both in the case of the model molecules and the complexes.

The analysis of the calculated results can support the experimental measures for the characterization of the metal environment and for investigating the metal and ligand content of the excited states. The joint analysis of the ligand K edge and metal L edge spectral features gives important insight into the covalency of the metal−ligand bond, because the intensities of the pre-edge structures can be related to the mixing of p ligand and d metal orbitals.

Acknowledgment. This work has been supported by grants from MIUR (Programmi di Ricerca di Interesse Nazionale COFIN ex 40% and FIRB) of Italy. A generous INSTM grant of computer time on the IBM SP4 supercomputer of CINECA (Bologna, Italy) is gratefully acknowledged.

References and Notes

(1) George, G. N.; Kipke, C. A.; Prince, R. C.; Sunde, R. A.; Enemark, J. H.; Cramer, S. P. *Biochemistry* **1989**, *28*, 5075.

(2) Kisker, C.; Schindelin, H.; Pacheco, A.; Wehbi, W. A.; Enemark, J. H.; Rees, D. C. *Cell* **1997**, *91*, 973.

(3) Hille, R. *Chem. Rev.* **1996**, *96*, 2757.

(4) Izumi, Y.; Glaser, T.; Rose, K.; McMaster, J.; Basu, P.; Enemark, J. H.; Hedman, B.; Hodgson, K. O.; Solomon, E. I. *J. Am. Chem. Soc.* **1999**, *121*, 10035.

(5) Xiao, Z.; Bruck, M. A.; Doyle, C.; Enemark, J. H.; Grittini, C.; Gable, R. W.; Wedd, A. G.; Young, C. G. *Inorg. Chem.* **1995**, *34*, 5950.

(6) Wang, H.; Peng, G.; Miller, L. M.; Scheuring, E. M.; George, S. J.; Chance, M. R.; Cramer, S. P. *J. Am. Chem. Soc.* **1997**, *119*, 4921.

(7) Wang, H.; Patil, D. S.; Gu, W.; Jacquamet, L.; Friedrich, S.; Funk, T.; Cramer, S. P. *J. Electron Spectrosc. Relat. Phenom.* **2001**, *114*, 855.

(8) Wang, H.; Ralston, C. Y.; Patil, D. S.; Jones, R. M.; Gu, W.; Verhagen, M.; Adams, M.; Ge, P.; Riordan, C.; Marganian, C. A.; Mascharak, P.; Kovacs, J.; Miller, C. G.; Collins, T. J.; Brooker, S.; Croucher, P. D.; Wang, K.; Stiefel, E. I.; Cramer, S. P. *J. Am. Chem. Soc.* **2000**, *122*, 10544.

(9) Rose, K.; Shadle, S. E.; Eidsness, M. K.; Kurtz, D. M.; Scott, R. A.; Hedman, B.; Hodgson, K. O.; Solomon, E. I. *J. Am. Chem. Soc.* **1998**, *120*, 10743.

(10) Glaser, T.; Hedman, B.; Hodgson, K. O.; Solomon, E. I. *Acc. Chem. Res.* **2000**, *33*, 859.

(11) Anxolabehere-Mallart, E.; Glaser, T.; Frank, P.; Aliverti, A.; Zanetti, G.; Hedman, B.; Hodgson, K. O.; Solomon, E. I. *J. Am. Chem. Soc.* **2001**, *123*, 4444.

(12) Zangwill, A.; Soven, P. *Phys Rev. A* **1980**, *21*, 1561.

(13) Levine, Z. H.; Soven, P. *Phys. Rev. A* **1984**, *29*, 625.

(14) van Gisbergen, S. J. A.; Snijders, J. G.; Baerends, E. J. *Comput. Phys. Commun.* **1999**, *118*, 119.

(15) Jamorski, Ch.; Casida, M. E.; Salahub, D. R. *J. Chem. Phys.* **1996**, *104*, 5134.

(16) Bauernschmitt, R.; Ahlrichs, R. *Chem. Phys. Lett.* **1996**, *256*, 454.

(17) Bauernschmitt, R.; Häser, M.; Treutler, O.; Ahlrichs, R. *Chem. Phys. Lett.* **1997**, *264*, 573.

(18) Stener, M.; Fronzoni, G.; de Simone, M. *Chem. Phys. Lett.* **2003**, *373*, 115.

(19) Casida, M. E. *Recent Advances in Density-Functional Methods*; World Scientific: Singapore, 1995; p 155.

(20) Gross, E. K. U.; Kohn, W. *Adv. Quantum Chem.* **1990**, *21*, 255.

(21) Baerends, E. J.; Ellis, D. E.; Roos, P. *Chem. Phys.* **1973**, *2*, 41.

(22) Fonseca Guerra, C.; Snijders, J. G.; te Velde, G.; Baerends, E. J. *Theor. Chem. Acc.* **1998**, *99*, 391.

(23) Van Leeuwen, R.; Baerends, E. J. *Phys. Rev. A* **1994**, *49*, 2421.

(24) Vosko, S. H.; Wilk, L.; Nusair, M. *Can. J. Phys.* **1980**, *58*, 1200.

(25) Tronc, M.; Dezarnaud-Dandine, C. *Chem. Phys. Lett.* **1991**, *184*, 267.

(26) Evans, J.; Mosselmans, F. W. *J. Phys. Chem.* **1991**, *95*, 9673.

(27) de Groot, F. M. F.; Hu, Z. W.; Lopez, M. F.; Kaindl, G.; Guillot, G.; Tronc, M. *J. Chem. Phys.* **1994**, *101*, 6570.